Intradental mechano-nociceptors serve as sentinels that prevent tooth damage

Elizabeth A. Ronan[1], Akash R. Gandhi[1], Brian S. C. Constantinescu[1], Karin H. Uchima Koecklin[1,2], Mak E. Guenther[1], Maximilian Nagel[3], Kaitlyn J. Blumberg[1], Tomer Stern[1], Peng Li[1,2], Joshua J. Emrick[1,*]

[1]Department of Biologic and Materials Sciences & Prosthodontics, School of Dentistry, University of Michigan, Ann Arbor, MI, USA.

[2]Life Sciences Institute, University of Michigan, Ann Arbor, MI, USA

[3]Sensory Cells and Circuits Section, National Center for Complementary and Integrative Health, Bethesda, MD, USA

*To whom correspondence should be addressed: jjemrick@umich.edu

ABSTRACT

Pain is the anticipated output of the trigeminal sensory neurons that innervate the tooth's vital interior[1,2]; however, the contribution of intradental neurons to healthy tooth sensation has yet to be defined. Here, we employ in vivo Ca^{2+} imaging to identify and define a population of myelinated high-threshold mechanoreceptors (intradental HTMRs) that detect superficial structural damage of the tooth and initiate jaw opening to protect teeth from damage. Intradental HTMRs remain inactive when direct forces are applied to the intact tooth but become responsive to forces when the structural integrity of the tooth is compromised, and the dentin or pulp is exposed. Their terminals collectively innervate the inner dentin through overlapping receptive fields, allowing them to monitor the superficial structures of the tooth. Indeed, intradental HTMRs detect superficial enamel damage and encode its degree, and their responses persist in the absence of either PIEZO2 or $Na_V1.8$[3,4]. Optogenetic activation of intradental HTMRs triggers a rapid, jaw opening reflex via contraction of the digastric muscle. Taken together, our data indicate that intradental HTMRs serve as sentinels that guard against mechanical threats to the tooth, and their activation results in physical tooth separation to minimize irreversible structural damage. Our work provides a new perspective on the role of intradental neurons as protective rather than exclusively pain-inducing and illustrates additional diversity in the functions of interoreceptors.

INTRODUCTION

Mammals instinctively use their teeth for mechanical behaviors including chewing to initiate digestion and biting for prey capture and self-defense. The protection and maintenance of enamel and teeth are essential when teeth do not regenerate as in humans. Loss of teeth is associated with poorer diet and nutritional status[5] as well as early mortality[6]. The somatosensory neurons within the trigeminal ganglion extend processes into the oral and

craniofacial tissues, including the inner tooth. Broadly, activation of primary sensory cells and their downstream neuronal targets produces outputs including sensorimotor reflexes[7,8] and perceptions of touch, temperature, body position, and pain. While we assume that the activation of tooth innervation is the source of substantial pain[9], whether tooth-innervating somatosensory neurons (hereafter intradental neurons) might contribute to the protection of tooth structure in health has not been explored.

Historically, intradental innervation is thought to arise from both myelinated (Aβ/Aδ) and unmyelinated (C-type) trigeminal sensory neurons. However, myelinated intradental neurons predominate based on immunohistochemical labeling[10], and transcriptomic analyses indicating the majority of intradental neurons express *S100b*, a marker of myelinated somatosensory neurons[11,12]. While electrophysiological experiments have demonstrated that fibers with conduction velocities in the Aδ range spike in extreme conditions when the inner tooth has been exposed[13], the molecular identity of intradental neurons and their capacity to respond in an intact tooth has not been explored. The combination of transcriptomic analyses with in vivo functional imaging provides a new ability to relate molecular identity with cell function[7,11,14–18]. Indeed, these tools have revealed the basis for touch sensation in the skin[12,19], and provide great potential for defining the role of intradental neurons.

Here, we develop a strategy to identify intradental neurons in the trigeminal ganglion without damaging the tooth, then monitor their response profiles to mechanical stimulation. We determined most responding neurons are large diameter and express transcriptomic markers of myelinated mechano-nociceptors (i.e., *S100b*, *Scn10a*, and *Calca*). These intradental neurons do not encode any direct forces applied to the intact outer tooth but are activated once the dentin has been exposed. Intradental terminal endings extend into the inner dentin providing an anatomical basis for their observed dentin-response profile. Importantly, we show

that intradental neurons represent a population of high-threshold mechanonociceptors (HTMRs) that collectively respond to superficial damage to the tooth. Damage responses persist in the absence of *Piezo2* further indicating intradental neurons represent HTMRs. Furthermore, direct optogenetic activation of intradental HTMRs induces digastric muscle contractions and evokes a protective jaw opening response that physically separates the opposing teeth. This work provides a new perspective on intradental neuron function by providing the sensory foundation for tooth protection, which involves the detection of superficial damage and the reflexive protection of the tooth.

RESULTS

Identification of large diameter intradental neurons in vivo through electrical stimulation of the intact tooth

To enable functional evaluation of intradental neurons, we adapted an in vivo trigeminal Ca^{2+} imaging technique in mice to visualize real-time activity of sensory neurons[7,20] while stimulating individual molars (Figure S1A-C). Past work in large mammals indicates that electrical stimulation applied to exposed dentin can elicit single unit responses within the alveolar nerve[21]. Furthermore, the electric pulp test is routinely used in clinical dentistry to assess tooth sensation in human patients. Thus, we reasoned that low voltage pulses delivered to the occlusal surface of individual intact molar teeth may identify corresponding intradental neurons. Electrical stimulation of molar 1 or molar 2 (2-4 V, 0.6 Hz, 200 ms, Figure 1A, see Methods) resulted in stereotyped phasic, transient Ca^{2+} responses from separate groups of trigeminal sensory neurons (Figure 1B-D, S1C) indicating discrete sensory inputs from each tooth. In each experimental iteration, we identified pulsing neurons (9-21 neurons, n=10, Figure 1E) on the surface of the ganglion (Figure S1C) with large diameters (46.4 ± 0.1

µm, n=99 neurons, Figure 1F) consistent with the upper range of somas of Aδ myelinated sensory neurons. These neurons also responded to direct application of Endo-Ice to the tooth surface, another clinical assay used to test human tooth pulp sensitivity[22] (Figure S1D). To confirm that electrical stimulation preferentially activates intradental neurons, we performed retrograde labeling (CTB-AF555) to ipsilateral mandibular molars 1 and 2[23] prior to Ca^{2+} imaging. This allowed us to confirm that the majority of CTB+ neurons demonstrated pulsed responses (81/111, 4 mice, Figure 1G-I). Taken together we have established an in vivo method to identify intradental neurons within an intact tooth enabling molecular and functional evaluation.

Intradental neurons express markers of putative HTMRs

We next sought to determine the molecular identity of electrically-activated intradental neurons. Our prior retrograde labeling opens the possibility that intradental neurons represent mechanoreceptors based on their transcriptomic classification[23]. To this end, we performed Ca^{2+} imaging followed by post-hoc in situ hybridization of whole mount dissected trigeminal ganglion[12]. We used a defined panel of probes (*S100b*, *Scn10a*, *Calca*, and *Mrgprd*) to delineate mechanoreceptor subtypes[12]. We utilized an AAV-based strategy to induce simultaneous GCaMP6f and mCherry expression in trigeminal sensory neurons. mCherry expression provided reliable guideposts for image alignment (Figure S1H) to match in situ hybridization staining (Figure S1I) with fluorescence responses from Ca^{2+} imaging. In line with our prior work, we determined that most responding intradental neurons expressed *Scn10a, Calca*, and *S100b* (31/47) suggesting these cells are nociceptive large diameter, myelinated HTMRs[12] (Figure 1J). Conversely, intradental neurons lacked expression of *Mrgprd* (1/47), a marker of unmyelinated C-type HTMRs[12]. Furthermore, 11/47 intradental neurons were marked by only *S100b*, suggesting few are likely to represent low-threshold mechanoreceptors

(LTMRs). Together these results demonstrate that intradental neurons captured by our paradigm primarily represent myelinated nociceptive HTMRs.

Intradental neurons respond to direct force after enamel removal

As intradental neurons express transcriptional markers of HTMRs, we next set out to determine their responses to mechanical forces directed to the intact tooth. We first tested whether intradental neurons respond to a range of noxious to innocuous forces applied to the enamel surface (0.4 - 20 g. Interestingly, we found that none of the intradental neurons as identified by electrical stimulation were activated by the mechanical forces tested (Figure 2A-B). As pressure applied to exposed inner tooth elicits responses in humans in the clinical setting[24], we reasoned that intradental neurons might detect these mechanical forces in exposed teeth. To test this, we evaluated responses to application of force before and after exposing the dental pulp. As expected, we found that intradental neurons were not activated by the mechanical force on the intact tooth (Figure 2D). Interestingly, in the same tooth after the dental pulp was exposed, a portion of intradental neurons now responded to mechanical stimulation (9/54, 17% of electrical responders, Figure 2D, F). To our surprise, in teeth where only the dentin was exposed, direct mechanical force now elicited responses from the majority of intradental neurons (32/41, 78% of electrical responders, Figure 2E, F). From these experiments, we conclude that intradental neurons are HTMRs (intradental HTMRs) that do not contribute to any direct forces applied to the intact tooth but respond to mechanical force after the removal of enamel.

Intradental HTMRs terminate in the tooth pulp and inner dentin

Our experiments testing direct force on tooth structures suggest the presence of terminal endings within the dentin, as mechanical stimulation of exposed dentin recruits a large

number of intradental neurons. We applied genetic strategies relying on *S100b* and *Scn10a* to drive fluorescent labeling of intradental HTMRs to visualize their terminal endings. While *S100b* delineates myelinated somatosensory neurons, it is also broadly expressed in the nervous system as well as non-neuronal peripheral cells. To restrict fluorescent labeling to *S100b*+ somatosensory neurons we crossed *S100b*-Cre into a Cre-dependent neuronal specific reporter strain (*Snap*25-LSL-2A-eGFP). We found dense GFP+ innervation of the coronal pulp as well as parallel GFP+ terminals penetrating to the inner 3rd of the dentin (Figure S2A-I). As *Scn10a* expression is highly restricted to sensory neurons, we repeated immunohistochemical experiments in teeth obtained from *Scn10a*-Cre; Ai32 mice (*Scn10a*-Cre; LSL-YFP). Here, we observed remarkably similar YFP+ innervation patterns within the pulp and inner dentin (Figure S2J-O). While these studies indicate that dentin is uniformly innervated by endings stemming from intradental neurons, the endings of individual neurons were not yet discerned. To generate sparse labeling of terminal endings we turned to AAV-based strategies that offer lower transduction efficiency[25] (Figure S3A-D). Here, AAV injections into either *S100b*-Cre and *Scn10a*-Cre mice achieved labeling of few intradental neurons to reveal terminal patterns within the dentin. Fluorescently-labeled fibers (*S100b*-tdT and *Scn10a*-GFP) were localized to only a portion of the overall dentin typically within a single pulp horn (Figure 2G, H) and exhibited tuft-like patterning penetrating into non-contiguous dentinal tubules. These findings indicate that single neurons target several tubules and multiple neurons are likely to innervate a local region of the inner dentin. With our sparse labeling, we also noted that terminal morphology appeared as a series of puncta running in parallel along the length of dentin tubules (Figure 2G, H). Taken together, we establish that intradental HTMRs, as defined by expression of *S100b* and *Scn10a*, contribute intermingled terminals to create dense innervation of the inner dentin.

Intradental HTMRs function to detect tooth enamel damage

Intradental HTMRs respond to mechanical stimulation following dentin exposure, providing input *after* the inner layers of the tooth have been exposed. We next sought to explore if these neurons also activate *while* molar teeth are damaged. To this end, we monitored responses of trigeminal sensory neurons while simultaneously damaging the enamel surface using a dental bur. We found that most intradental HTMRs responded to cutting of the surface enamel (64/70, 91%, n = 4). We next tested a range of vibration frequencies (50 - 200 Hz) applied to the tooth. Minimal activity was observed from intradental HTMRs (2/52, 3%, Figure S4B-E) indicating these cells detect enamel cutting. Taken together, these experiments indicate that intradental HTMRs encode damaging mechanical stimulation of individual teeth.

Intradental HTMRs detect superficial frictional damage of the tooth surface and encode damage severity

The cutting of the exterior tooth produced overt damage of the enamel layer (Figure S4A) and triggered a response from intradental HTMRs. Does the response profile of these neurons provide information about the degree of tooth damage? To this end we sought to introduce a stimulus that creates lesser damage by removing the carbide flutes from the dental bur. This “fluteless” bur produces friction, but not perceptible damage (Figure S4A). Remarkably, friction on the surface of the tooth triggered activation of almost half of the intradental HTMRs identified by electrical stimulation (98/205, 47%, n = 7 mice, Figure 3A, B). Subsequently, the cutting stimulus evoked responses in these 98 neurons in addition to recruiting responses from 58 additional intradental HTMRs (156/205, 76%, n = 7 mice, Figure 3C). Interestingly, friction triggered smaller magnitude responses compared to cutting,

suggesting that intensity of activation increases with degree of tooth damage (Figure 3H). Post hoc in situ confirmed that intradental HTMRs that respond to tooth cutting were largely *Scn10a*+ (22/27 neurons, 82%, n = 4 mice, Figure 3E). We found that cutting and friction produced equivalent, minimal warming of the inner tooth (<3ºC, Figure S4F-H) that is unlikely to trigger any response and cannot account for our observed differences between response magnitude. These results demonstrate that intradental HTMRs detect superficial frictional damage and encode the degree of damage.

Damage responses of intradental HTMRs are independent of *Piezo2* or *Scn10a* ($Na_V1.8$)

Our previous work indicated that intradental neurons express the mechanosensitive ion channel *Piezo2*[23] that underlies mechanosensation in the skin[12,26]. Is PIEZO2 required for intradental HTMR activation by enamel cutting? To investigate this and circumvent lethality of global *Piezo2* deletion, we examined neuron responses to cutting in mice with AAV-mediated conditional knock out of *Piezo2* (Piezo2-cKO). To confirm recombination in sensory neurons and functional loss of PIEZO2[12,17], we ensured Ca^{2+} responses to innocuous cheek brush were lost while responses to cheek pinch were maintained (Figure S4I). However, even in the context of Piezo2-cKO, we observed no significant change in the proportion of intradental HTMRs responding to cutting (Figure 3F, H). These findings indicate that *Piezo2* is not required for the neuronal detection of enamel damage, further supporting their identity as intradental HTMRs.

Intradental HTMRs are marked by *Scn10a* expression, encoding the pore-forming alpha subunit of $Na_V1.8$ which contributes to noxious mechanical pain[4]. We next sought to determine whether *Scn10a* is required for intradental HTMR sensory transduction in response to enamel damage. To this end, we examined neuronal responses in the well-established knock in/knock

out Scn10a-Cre driver strain[27]. As expected, *Scn10a*-Cre enabled capture of intradental HTMRs with nearly equivalent counts and proportion of cutting responders compared to initial unbiased AAV-mediated recombination (Figure S5A-C). However, in homozygotes where *Scn10a* is replaced by Cre expression, we found no reduction in the proportion of intradental HTMRs responding to enamel cutting compared to other strains (Figure 3G, H). These experiments indicate that the *Scn10a* gene product ($Na_v1.8$) is not required for the transduction of damage responses. Taken together, these experiments suggest a role for an unknown high-threshold mechanical receptor in intradental HTMRs that detects superficial damage of the teeth.

Activation of intradental HTMRs induces digastric muscle contraction and initiate protective jaw opening

Considering teeth are at risk for damage during regular function, we next sought to determine how activation of the intradental HTMRs might drive protective responses. Somatosensory HTMRs are known to initiate reflexes to protect structures from damage[7]. Interestingly, low intensity electrical stimulation of teeth in larger mammals has been shown to elicit electromyogram (EMG) activity in some muscles of mastication[28]. Indeed, we first confirmed that electrical stimulation of the inferior alveolar nerve (IAN) elicited EMG activity in the anterior digastric muscle (Figure S6A) which contributes to jaw opening (i.e., mandibular deflection). We next sought to determine if selective activation of intradental neurons was capable of inducing EMG activity in the anterior digastric muscle. To this end, we relied on AAV-Cre transduction of intradental neurons via cavitations in the molar teeth to initiate the expression of channelrhodopsin-2 (ChR2) in a Cre-dependent effector strain (Ai32, Figure 4A, S6B). Activation of intradental neurons expressing ChR2+ using blue light stimulation (15 ms pulse) of the trigeminal ganglion produced an immediate, transient waveform in the ipsilateral

anterior digastric EMG (Figure 4B-C, S6C, E-G; 0.97 +/- 0.3 mV amplitude). Alternatively, we found no EMG activity in response to blue light stimulation when intradental neurons were ChR2-. The ipsilateral masseter muscle that contributes to closing the jaw also failed to demonstrate EMG activity after light stimulation in either condition (Figure 4B, S6E). Prolonged blue light stimulation (100 ms pulse) elicited similar waveforms in ipsilateral digastric EMG (Figure S6D-G; $p>0.05$). Of note, changes in EMG activity were never observed at light offset (Figure 4B, S6C,D). Taken together, these data indicate that somatic activation of intradental neurons leads to electrical activity of the anterior digastric muscle.

The anterior digastric muscles function to open the jaw by depressing the mandible[29]. To directly determine if collective activation of intradental HTMRs initiates overt jaw movement, we next employed a genetic strategy to drive ChR2 expression in these cells using *Scn10a*-Cre. For these experiments, we selectively activated intradental HTMRs by directing our optical fiber onto a single intact molar tooth. Here, we found that pulses of blue light (470 nm, 1s) elicited a rapid, brief mandibular deflection (10 ms onset, reversing after 30 ms, Figure 4E). Paralleling EMG activity, light offset had no effect on jaw position. We determined that repeated blue light pulses (10 pulses, 0.5 Hz, 1s) induced a series of mandibular deflections entrained to light onset (Figure 4F) that did not diminish between pulse trains (Figure 4F-G, S6H), average deflection 305 +/- 37 vs 289 +/- 49 µm, $p>0.05$). Conversely, green light (545 nm) failed to produce any jaw movements despite identical stimulating frequency and duration (10 pulses, 0.5 Hz, 1s). Importantly, blue light stimulation of molar-adjacent tissues (i.e. hard palate or oral vestibule) also failed to produce any jaw movements (Figure 4F). Taken together, these experiments reveal that activation of intradental HTMRs drives a rapid jaw opening that physically disengages the teeth from an insult.

DISCUSSION

Mammalian teeth are specialized internal organs that endure a range of mechanosensory stimuli during biting and mastication. While intradental neurons are known to evoke pain through their activation, a biological role has not been defined for this interoceptive innervation using modern approaches. Here, we establish an in vivo functional imaging approach to identify intradental neurons in an intact tooth, define their responses to mechanical damage of the tooth, and determine that their targeted activation leads to jaw opening. Our experiments reveal a uniform population of intradental HTMRs that 1) detect forces applied to the exposed dentin as well as damage of the superficial enamel, 2) do not contribute to the detection of innocuous forces encountered by the tooth, 3) target the inner dentin with intermingled terminals providing anatomical evidence supporting their coordinated response to stimuli, 4) rely on a Piezo2-independent mechanism to transduce damage responses, and 5) drive digastric muscle contraction and a protective jaw opening reflex.

Protective reflexes have been described for the knee (patellar reflex), cornea (eye-blink reflex) and the jaw (jaw-jerk reflex) that occur within 100 ms latencies. Here, we describe an extremely rapid reflex (5-15 ms) that is initiated following the activation of terminals of intradental HTMRs within the dentin. We predict that the intradental HTMRs respond when the tooth makes unexpected contact with hard foods (i.e., cartilage or bone) or opposing teeth. Based on our data, activation of intradental HTMRs within a single tooth during mastication would be sufficient to drive a reflex response that would halt jaw closure. Intradental HTMRs efficiently respond to damage of the tooth indicating they may be tuned for its detection; however, the precise component of the damage stimulus that triggers intradental HTMR responses will be difficult to determine considering the miniature size of the mouse tooth. We

expect that comparing structural changes in the tooth caused by vibration and cutting could reveal the activating component.

Recent work indicates that *Calca*+ circumferential-HTMRs (circ-HTMRs) innervating hair follicles in skin mediate a nocifensive response[7]. Intradental HTMRs also represent a population of *Calca*/CGRP+ population of somatosensory neurons that mediate a reflexive, protective response. While CGRP+ neurons have been further subdivided within the skin based on their expression patterns, none feature terminal morphology exhibited by the intradental HTMRs[19]. Functionally, intradental HTMRs share the response profile of some subsets of CGRP+ HTMRs including *Smr2*+ and *Bmpr1b*+ somatosensory neurons. We anticipate that intradental HTMRs may diverge in their thermal response profiles considering their position within the insulated tooth structure. It is yet to be determined if intradental HTMRs represent a new subclass of CGRP+ HTMRs that innervate and protect other vulnerable tissue structures by engages withdrawal reflexes.

Intradental neurons have been previously suggested to function as LTMRs[30] which is consistent with their expression of Piezo2. On the contrary, our data directly shows that intradental neurons fail to respond to direct forces or vibration applied to the intact tooth. It is highly probable that light forces applied to the teeth are transduced by LTMRs innervating surrounding periodontal (i.e., tooth surrounding) tissues. Future studies investigating the molecular identity and innervation targets within surrounding periodontium tissues will shed insight into how direct mechanical forces applied to the tooth are sensed.

We determined that damage responses by intradental neurons are independent of the canonical mechanoreceptor PIEZO2 as well as a nociceptive transducer $Na_V1.8$. Our data suggest that blocking either ion channel is unlikely to prevent activation of the intradental

neurons as they are structurally damaged. This is in contrast to a recent clinical trial that supports the effectiveness of inhibition of $Na_v1.8$ to diminish post-surgical inflammatory pain[31]. Instead, we propose the existence of unidentified molecular sensors for high threshold mechanical stimulation of the tooth. Single-cell sequencing of intradental neurons[32] toward screening and identification of novel high-threshold mechanoreceptors and nociceptive transducers will provide additional targets for next-generation dental anesthetics that can be validated with our approach.

While some evidence suggests that the tooth pulp receives innervation from C-fiber nociceptors that contribute to forms of tooth-related pain, our work to-date suggests these are unlikely to contribute to the protective reflex response. Our findings do not exclude the possibility that C-fibers may be present deep in the tooth pulp where they could contribute to differential aspects of tooth physiology such as in the context of inflammation. Clinically, we predict intradental HTMRs may underlie acute pain during biting as part of cracked tooth syndrome[33]. Further work will be needed to determine if responses of intradental HTMRs are altered by the inflammatory milieu. For instance, intradental HTMRs may exhibit lower threshold responses to mechanical stimulation in the context of tooth decay, and begin to contribute to the exquisite pain associated with the colloquial toothache.

While our study indicates that intradental HTMRs respond to damage and initiate an important protective reflex, others behavioral outputs resulting from their activation has yet to be explored. We anticipate that excessive or persistent activation of intradental HTMRs may be sufficient to elicit pain behaviors in mice, and could be the basis for defining additional orofacial movements that indicate the experience of pain. Further experiments will be necessary to understand if the jaw-opening reflex and pain are necessarily concurrent or may be uncoupled in freely-behaving animals.

REFERENCES

1. Henry, M. A. & Hargreaves, K. M. Peripheral Mechanisms of Odontogenic Pain. *Dental Clinics of North America* **51**, 19–44 (2007).
2. Renton, T. Dental (Odontogenic) Pain. *Rev Pain* **5**, 2–7 (2011).
3. Murthy, S. E. *et al.* The mechanosensitive ion channel Piezo2 mediates sensitivity to mechanical pain in mice. *Sci Transl Med* **10**, eaat9897 (2018).
4. Akopian, A. N. *et al.* The tetrodotoxin-resistant sodium channel SNS has a specialized function in pain pathways. *Nat Neurosci* **2**, 541–548 (1999).
5. Xu, K.-H. *et al.* Association of Tooth Loss and Diet Quality with Acceleration of Aging: Evidence from NHANES. *Am J Med* **136**, 773-779.e4 (2023).
6. Koka, S. & Gupta, A. Association between missing tooth count and mortality: A systematic review. *J Prosthodont Res* **62**, 134–151 (2018).
7. Ghitani, N. *et al.* Specialized Mechanosensory Nociceptors Mediating Rapid Responses to Hair Pull. *Neuron* **95**, 944-954.e4 (2017).
8. Barik, A., Thompson, J. H., Seltzer, M., Ghitani, N. & Chesler, A. T. A Brainstem-Spinal Circuit Controlling Nocifensive Behavior. *Neuron* **100**, 1491-1503.e3 (2018).
9. Slade, G. D. Epidemiology of dental pain and dental caries among children and adolescents. *Community Dent Health* **18**, 219–227 (2001).
10. Byers, M. R. & Cornel, L. M. Multiple complex somatosensory systems in mature rat molars defined by immunohistochemistry. *Archives of Oral Biology* **85**, 84–97 (2018).
11. Nguyen, M. Q., Wu, Y., Bonilla, L. S., von Buchholtz, L. J. & Ryba, N. J. P. Diversity amongst trigeminal neurons revealed by high throughput single cell sequencing. *PLoS ONE* **12**, e0185543 (2017).

12. von Buchholtz, L. J. *et al.* Decoding Cellular Mechanisms for Mechanosensory Discrimination. *Neuron* **109**, 285-298.e5 (2021).
13. Närhi, M. V., Hirvonen, T. J. & Hakumäki, M. O. Activation of intradental nerves in the dog to some stimuli applied to the dentine. *Arch Oral Biol* **27**, 1053–1058 (1982).
14. von Buchholtz, L. J., Lam, R. M., Emrick, J. J., Chesler, A. T. & Ryba, N. J. P. Assigning transcriptomic class in the trigeminal ganglion using multiplex in situ hybridization and machine learning. *Pain* **161**, 2212–2224 (2020).
15. Sharma, N. *et al.* The emergence of transcriptional identity in somatosensory neurons. *Nature* **577**, 392–398 (2020).
16. Usoskin, D. *et al.* Unbiased classification of sensory neuron types by large-scale single-cell RNA sequencing. *Nat Neurosci* **18**, 145–153 (2015).
17. Servin-Vences, M. R. *et al.* PIEZO2 in somatosensory neurons controls gastrointestinal transit. *Cell* **186**, 3386-3399.e15 (2023).
18. Lam, R. M. *et al.* PIEZO2 and perineal mechanosensation are essential for sexual function. *Science* **381**, 906–910 (2023).
19. Qi, L. *et al.* A DRG genetic toolkit reveals molecular, morphological, and functional diversity of somatosensory neuron subtypes. 2023.04.22.537932 Preprint at https://doi.org/10.1101/2023.04.22.537932 (2023).
20. Yarmolinsky, D. A. *et al.* Coding and Plasticity in the Mammalian Thermosensory System. *Neuron* **92**, 1079–1092 (2016).
21. Virtanen, A., Närhi, M., Huopaniemi, T. & Hirvonen, T. Thresholds of intradental A-and C-nerve fibres in the cat to electrical current pulses of different duration. *Acta Physiologica Scandinavica* **119**, 393–398 (1983).
22. Chen, E. & Abbott, P. V. Dental Pulp Testing: A Review. *Int J Dent* **2009**, 365785 (2009).

23. Emrick, J. J., von Buchholtz, L. J. & Ryba, N. J. P. Transcriptomic Classification of Neurons Innervating Teeth. *J Dent Res* **99**, 1478–1485 (2020).
24. Wanachantararak, S., Ajcharanukul, O., Vongsavan, N. & Matthews, B. Effect of cavity depth on dentine sensitivity in man. *Arch Oral Biol* **66**, 120–128 (2016).
25. Byers, M. R. & Calkins, D. F. Trigeminal sensory nerve patterns in dentine and their responses to attrition in rat molars. *Arch Oral Biol* **129**, 105197 (2021).
26. Szczot, M. *et al.* PIEZO2 mediates injury-induced tactile pain in mice and humans. *Sci Transl Med* **10**, eaat9892 (2018).
27. Stirling, C. L. *et al.* Nociceptor-specific gene deletion using heterozygous NaV1.8-Cre recombinase mice. *PAIN* **113**, 27 (2005).
28. Närhi, M., Virtanen, A., Hirvonen, T. & Huopaniemi, T. Comparison of electrical thresholds of intradental nerves and jaw-opening reflex in the cat. *Acta Physiol Scand* **119**, 399–403 (1983).
29. Perry, S. K. & Emrick, J. Trigeminal somatosensation in the temporomandibular joint and associated disorders. *Front. Pain Res.* **5**, (2024).
30. Dong, W. K., Chudler, E. H. & Martin, R. F. Physiological properties of intradental mechanoreceptors. *Brain Research* **334**, 389–395 (1985).
31. Jones, J. *et al.* Selective Inhibition of NaV1.8 with VX-548 for Acute Pain. *N Engl J Med* **389**, 393–405 (2023).
32. Lee, P. R. *et al.* Transcriptional profiling of dental sensory and proprioceptive trigeminal neurons using single-cell RNA sequencing. *Int J Oral Sci* **15**, 1–14 (2023).
33. Lynch, C. D. & McConnell, R. J. The cracked tooth syndrome. *J Can Dent Assoc* **68**, 470–475 (2002).

ACKNOWLEDGEMENTS

This work is supported by K22DE029779 (J.J.E.) and T32DE007057 (E.A.R.). We thank Dr. Nicholas Ryba for his feedback throughout this project and valuable comments on this manuscript. We thank Dr. Nima Ghitani for his technical assistance with in vivo imaging. We thank Dr. Alexander Chesler, Dr. Lauren Surface, and members of the Emrick lab for helpful comments and suggestions. We are grateful to donors of knockin mice for *S100b*-Cre knockin mice (Ryba); *Piezo2*-cKO knockin mice (Chesler); and *Snap25*-LSL-2A-EGFP-D knockin mice (Dr. Claire LePichon).

AUTHOR CONTRIBUTIONS

All authors gave final approval and agreed to be accountable for all aspects of the work. J.J.E. and E.A.R. conceptualized and directed the study. E.A.R., A.R.G., and J.J.E. performed Ca^{2+} imaging experiments with acquisition help from M.N. and B.S.C.C., and assistance in analysis from B.S.C.C. and T.S.. E.A.R., M.E.G., A.R.G., B.S.C.C, K.J.B., and J.J.E. performed survival surgeries and histological studies. K.H.U.K. performed optogenetic stimulation and EMG measurements, and analyzed the data. E.A.R., B.S.C.C., and J.J.E. performed optogenetic stimulation and mandibular deflection measurements. E.A.R., A.R.G., and J.J.E. interpreted the data, wrote the manuscript and generated figures with input from all other authors.

DECLARATION OF INTERESTS

Authors declare no competing interests.

FIGURES AND FIGURE LEGENDS

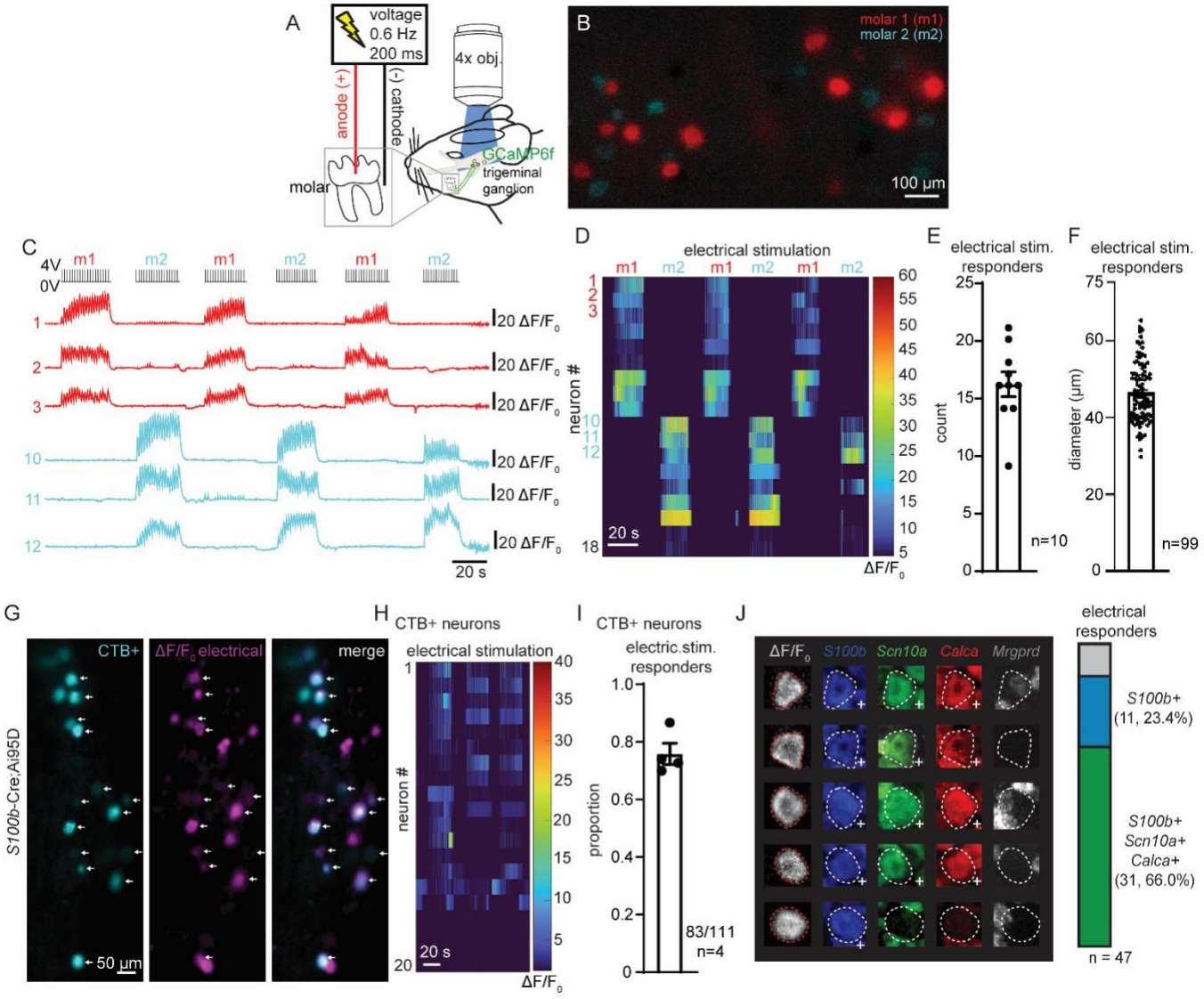

Figure 1. Functional imaging of intradental neurons reveals a large-diameter population of putative myelinated HTMRs.

(A) Schematic of methodology used to record in vivo sensory neurons in the trigeminal ganglion (TG) in response to stimulation of mouse molar tooth in the oral cavity. Intradental neurons were identified via delivery of low voltage pulses (4V, 0.6 Hz, 200 ms) to individual mandibular molars. Data in (A-E) were obtained from adult Ai95(RCL-GCaMP6f)-D (Ai95D) mice injected postnatally (P0-P3) with AAV9-Cre.

(B-D) Voltage stimulation enabled identification of intradental neurons innervating a single molar. (B) Imaging field showing merged single frames of Ca^{2+} response (ΔF/F0). Neurons with responses entrained to voltage pulses to either molar 1 (m1, red) or molar 2 (m2, cyan). Scale bar, 100µm. (C) Example raw traces of GCaMP6f signal from identified m1 (red) and m2 (cyan) intradental neurons. Numbers correspond to neurons circled in (B). Bars to the right of traces indicate 20 ΔF/F0. (D) Example heatmap from single TG showing in vivo GCaMP6f responses of 18 intradental neurons to voltage pulses. Neurons were grouped according to molar target of stimulation (m1 or m2). Stimuli used are indicated above the heatmap. Traces in (C) are designated neurons shown in (D).

(E) Bar graph showing the mean number of neurons per trial that responded to ≥2 voltage pulses, designating them as intradental. Plotted individual data points represent the number of responding neurons in separate imaging trials. Error bars indicate the SEM. n = 10 mice.

(F) Bar graph showing the mean diameter of neurons that responded to ≥2 voltage pulses, designating them as intradental. Plotted individual data points represent the number of responding neurons in separate imaging trials. Bar shows the mean value, and error bars indicate the SEM. n = 99 neurons from 7 mice.

(G-I) Retrograde labeling marks intradental neurons that are activated by electrical stimulation of the molars. Retrograde tracer CTB-AF555 was applied to small cavitations in mandibular molars (m1/m2) 16 hr prior to functional imaging. (G) Sample images depicting overlap of CTB labeling with Ca^{2+} response (ΔF/F0) of neurons responding to applied voltage pulses. Scale bar, 50µm. Left panel: CTB labeling; Middle panel: single frame (ΔF/F0) from recording during response to voltage pulse; Right panel: Merge. (H) Example heatmap showing responses of combined m1/m2 CTB+ neurons to voltage pulses. (I) Bar graph showing the proportion of CTB+ TG neurons that respond to ≥2 voltage pulses. Plotted individual data points represent

the calculated proportion of CTB+ cells that respond to ≥2 voltage pulses for each ganglion. Bar shows the mean and error bars indicate the SEM. n = 4 mice. CTB, cholera toxin B-subunit. Data in (G-I) were obtained from *S100b*-Cre; Ai95D mice. See Figure S1E-G for validation of *S100b*-Cre; Ai95D intradental neuron responses.

(J) Alignment of in vivo functional imaging responses with multiplexed whole-mount ISH enables molecular classification of intradental neurons. Data for all experiments were obtained from Ai95(RCL-GCaMP6f)-D (Ai95D) mice injected postnatally (P0-P3) with AAV9-hSyn1-mCherry-2A-iCre, enabling mCherry expression to serve as guideposts to align functional imaging with ISH images. (Left) Multiplexed whole-mount ISH staining following alignment to in vivo GCaMP6f fluorescence. Probes: s100 calcium-binding protein B (*S100b*, blue), alpha-Nav1.8 (*Scn10a*, green), calcitonin gene-related peptide (CGRP; *Calca*, red), mas-related G protein-coupled receptor member D (*Mrgprd*, white). Plus sign in bottom right of each subpanel indicates positive staining. (Right) Vertical bar (parts of a whole) indicates number and percentage of neurons expressing selected genes in intradental neurons. *S100b, Scn10a,* and *Calca* mark the majority of functionally-responding intradental neurons designating these as large diameter, myelinated nociceptors indicative of HTMRs (66.0%, 31/47 responding neurons). Most other neurons were *S100b*-positive labeled cells indicating large-diameter myelinated cells (23.4%, 11/47 responding neurons). n = 5 mice, comprising 47 intradental neurons.

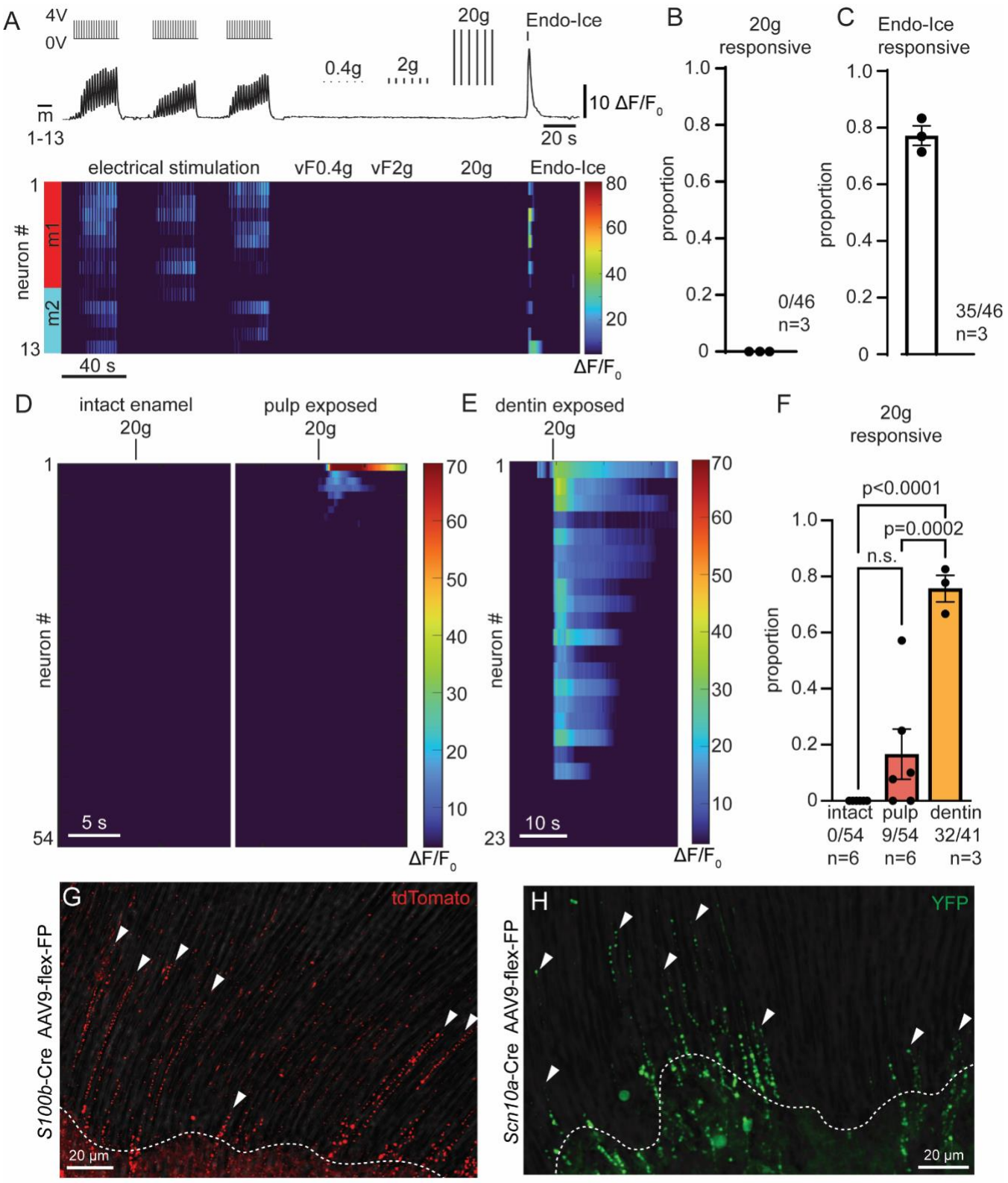

Figure 2. Intradental neurons are HTMRs that encode direct force after enamel removal and innervate the dental pulp and inner dentin

(A-C) Intradental neurons do not respond to direct forces applied to the intact tooth. (A) Example trace (top) and associated heatmap (bottom) showing absence of intradental neuron response to direct forces applied to the intact tooth, although they maintained responsiveness to Endo-Ice. Stimuli used are indicated above the traces. Bar to the right of trace indicates 10 ΔF/F0. (B) Bar graph showing proportion of intradental neurons that respond to direct force. Plotted individual data points represent the proportion of force responsive/intradental neurons per trial. Bar shows the mean and error bars indicate the SEM. n = 3 mice, comprising 46 cells. (C) Bar graph showing proportion of intradental neurons that respond to Endo-Ice. Plotted individual data points represent the proportion of Endo-Ice responsive/intradental neurons per trial. Bar shows the mean and error bars indicate the SEM. n = 3 mice, comprising 46 cells.

(D-F) Intradental neurons respond to direct forces following structural damage of the tooth. (D) Heatmap showing response profiles of 54 intradental neurons from 3 mice when direct force is applied to the tooth while intact (left) and following pulp exposure via removal of overlying enamel and dentin (right). (E) Example heatmap showing the response of intradental neurons to direct force applied to exposed dentin. (F) Bar graph showing proportion of direct force response/intradental neurons before and after two forms of tooth structural damage. Plotted individual data points represent the proportion of force responsive/intradental neurons per trial. Bar shows the mean and error bars indicate the SEM. n = 6 mice for intact enamel, n = 6 mice for pulp exposed, n = 3 mice for dentin exposed. p-values from one-way ANOVA with Tukey correction indicated with the graph. Data for D-F were obtained from Ai95(RCL-GCaMP6f)-D (Ai95D) mice injected postnatally (P0-P3) with AAV9-Cre.

(G) Representative image of immunostained neuronal terminals merged with brightfield image of dentin tubules in demineralized molars from *S100b*-Cre mice receiving TG injection of AAV9-flex-tdTomato to induce sparse labeling of trigeminal sensory neurons. Enamel, a fully

mineralized structure, has been removed completely by demineralization. This experiment was repeated in n = 5 mice. Scale bar: 20 µm.

(H) Representative image of immunostained neuronal terminals merged with brightfield image of dentin tubules in demineralized molars from *Scn10a*-Cre mice injected using a Cre-dependent AAV to induce sparce labeling of terminals (see methods). Enamel, a fully mineralized structure, has been removed completely by demineralization. This experiment was repeated in n = 4 mice with additional littermate and no primary controls. Scale bar: 20 µm.

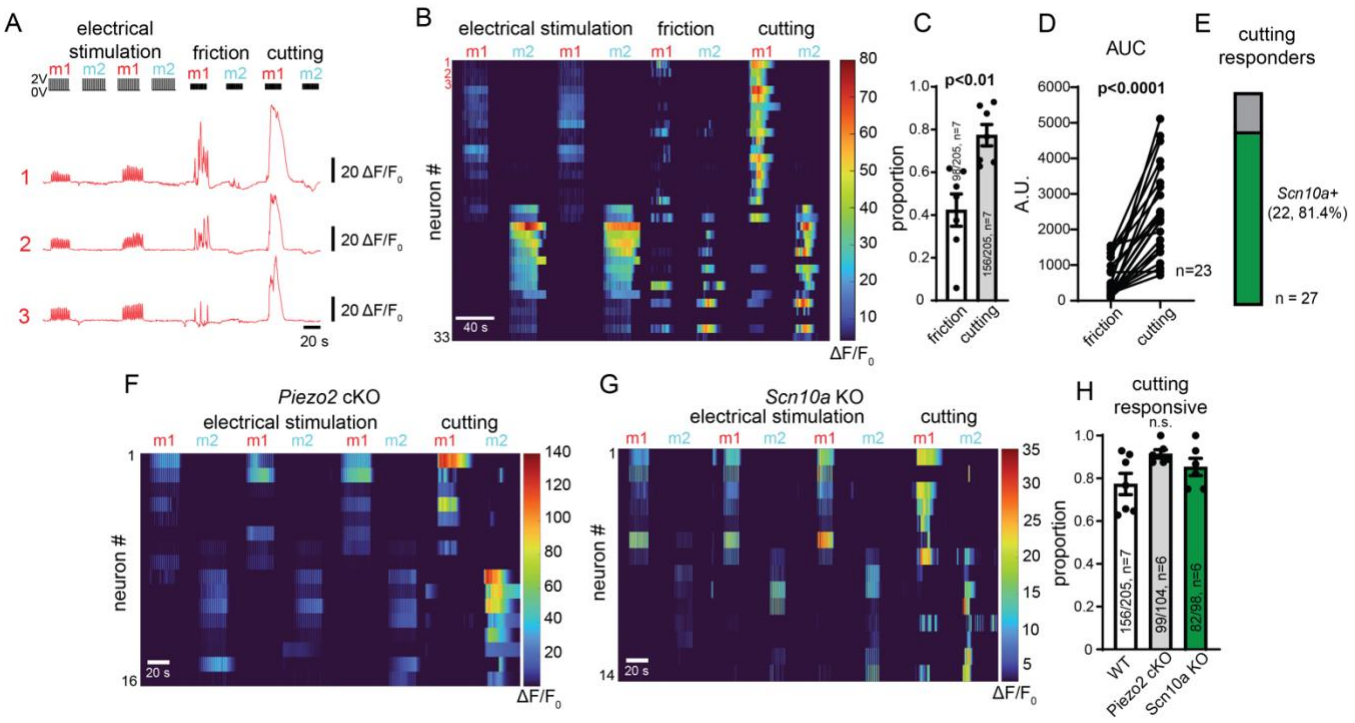

Figure 3. Intradental HTMRs detect enamel damage, independent of *Piezo2* or *Scn10a* ($Na_V1.8$).

(A-E) Intradental HTMRs sense cutting and superficial frictional damage of tooth enamel. (A) Example traces showing intradental neuron response to enamel cutting and friction applied to individual molars. Stimuli used are indicated above the traces. Bars to the right of traces indicate 20 ΔF/F0. (B) Example heatmap containing traces shown in (A). (C) Bar graph showing proportion of friction and cutting responsive intradental neurons identified by electrical stimulation. Plotted individual data points represent the proportion for each trial. Bar shows the mean and error bars indicate the SEM. n = 7 mice, comprising 205 total cells, $p<0.01$, Unpaired t-test. (D) Line graph depicting magnitude of Ca^{2+} responses of intradental neurons to friction versus cutting. Individual points represent calculated area under the curve (AUC) during designated stimulation for each cell. n = 23 cells, $p<0.0001$, Paired t-test. (E) Vertical

bar (parts of a whole) indicates number and percentage of cutting responsive neurons that express *Scn10a* (81.4%, 22/27 cutting responsive neurons, n = 4 mice). Results in E are cutting responses from primary data also used in Figure 1J.

(F) Example heatmap showing stereotypical intradental HTMR responses to cutting persist in *Piezo2*-cKO mice.

(G) Example heatmap showing stereotypical intradental HTMR responses to cutting persist in *Scn10a*-KO mice.

(H) Bar graph depicting the proportion of intradental HTMRs that respond to enamel cutting in wildtype, *Piezo2*-cKO, and *Scn10a*-KO mice. Plotted individual data points represent the calculated proportion of enamel cutting responsive/intradental neurons. Bar shows the mean, and error bars indicate the SEM. Intradental neurons were imaged from n = 6 or 7 adult mice per genotype. No significant differences were observed with $p>0.05$ using One-way ANOVA with Tukey's correction.

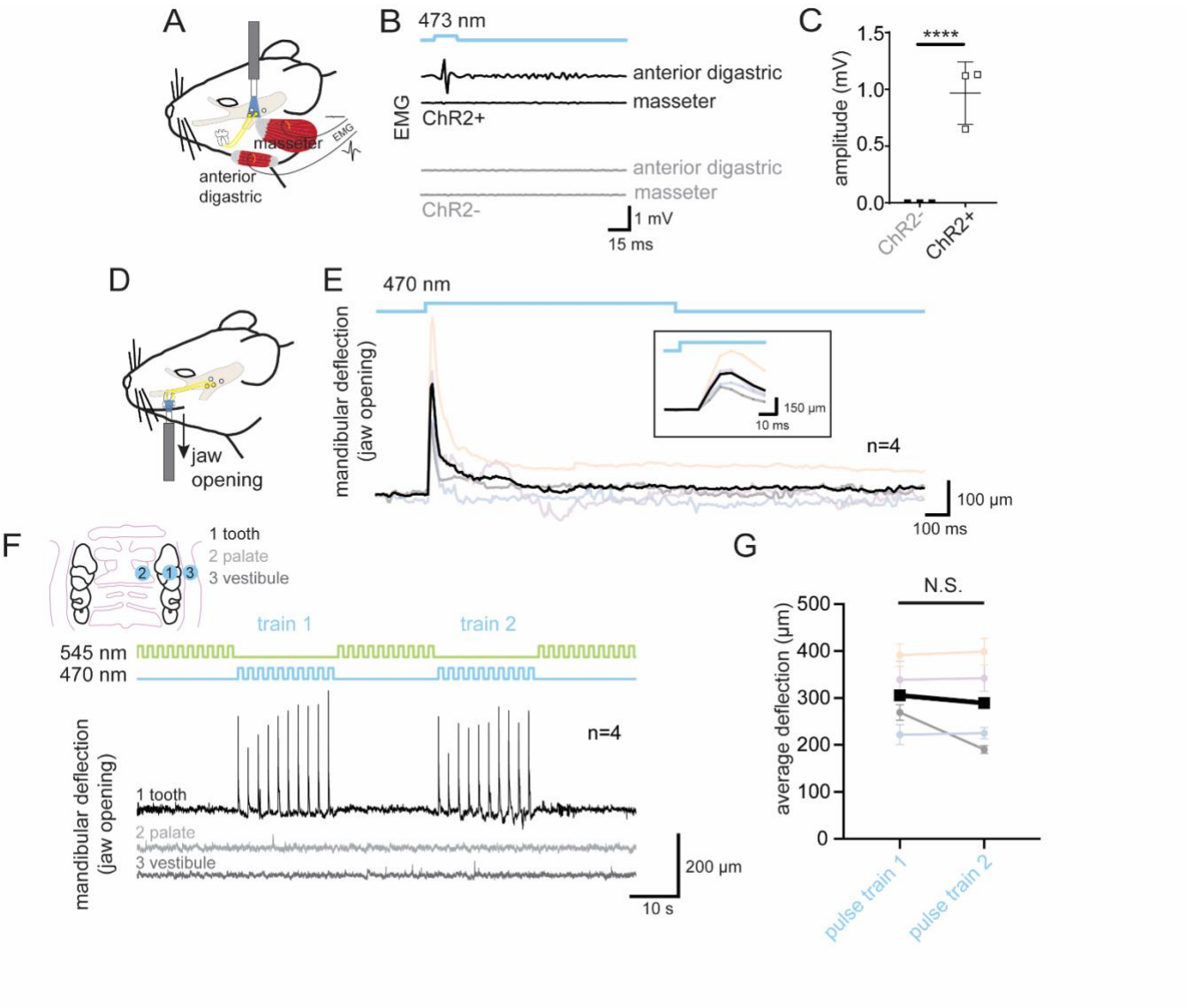

Figure 4. Optogenetic activation of intradental HTMRs induces digastric muscle activity and initiates a jaw opening reflex

(A-C) Optogenetic activation of intradental neurons induces activity in the anterior digastric muscle EMG. (A) Schematic demonstrating the experimental approach to selectively activate intradental neurons while recording EMG from the anterior digastric and masseter muscles. Channelrhodopsin-2 was selectively expressed in right mandibular intradental neurons innervating M1 and M2 molars via tooth injection of AAV6/2-hEF1a-iCre into Ai32(RCL-ChR2(H134R)/EYFP) mice. An optical fiber was implanted over the right trigeminal ganglia to

selectively activate intradental neurons while EMG signals of the ipsilateral anterior digastric or masseter muscles were recorded. (B) Example traces demonstrating EMG activity elicited by optogenetic activation of intradental neurons (15 ms, 473 nm). EMG activity is observed in the ipsilateral anterior digastric muscle, but not masseter muscle. Mice lacking channelrhodopsin-2 expression in intradental neurons show no changes in EMG activity for either the anterior digastric or the masseter muscles in response to blue light stimulation; n = 3 mice for all conditions. (C) Graph depicting the amplitude of activity of digastric muscle EMG in response to blue light stimulation (15 ms, 473 nm). Plotted individual data points represent the peak-to-peak amplitude of the elicited EMG trace. Error bar indicates SD. n = 3 mice per condition. Significant differences were observed between experimental (ChR2+) and control animals (ChR2-) with $p<0.0001$ using Unpaired t-Test.

(D-G) Optogenetic activation of intradental neuron terminals in the intact tooth results in mandibular deflection (i.e. jaw opening). (D) Schematic demonstrating the experimental approach. Channelrhodopsin-2 expression (Ai32) was driven by *Scn10a*-Cre. An optical fiber (500 µm) was positioned perpendicular to the surface of the first maxillary molar tooth or adjacent oral structures (hard palate or oral vestibule). Deflection was determined by monitoring the position of maxillary and mandibular incisors (see Methods). (E) Traces of average measured mandibular deflection in response to a single blue-light pulses (470 nm, 1s) directed to the molar tooth. Black trace represents the average (n = 4 mice). Multicolored traces represent average measurements from each mouse (n = 10 traces/mouse). Inset shows brief timescale of trace from (E) demonstrating kinetics of mandibular deflection in relation to light onset. (F) Average trace of measured mandibular deflection in response to trains of blue or green light pulses (470nm or 545nm, 10 pulses, 0.5 Hz, 1s) directed at oral structures. Sequential blue light pulses directed at the molar tooth (black trace), but not adjacent

structures (light and dark grey traces) induced mandibular deflection after each blue light onset. No jaw movements were observed in response to green light stimulation. (G) Line graph depicting average mandibular deflection in response to sequential blue light pulse train stimulation of molar. Average deflection from each mouse is plotted as multicolored individual points and represents mean peak amplitude and error bars show SEM of mandibular deflection during stimulation. n = 10 measurements per mouse per train related to traces shown in (F). Black points represent the average of n = 4 mice. $p>0.05$ using Unpaired t-Test.